Chemical Engineering Science 182 (2018) 28–43

Contents lists available at ScienceDirect

Chemical Engineering Science

journal homepage: www.elsevier.com/locate/ces

A liquid bridge model for spherical particles applicable to asymmetric configurations

Xiaosong Sun *, Mikio Sakai *

Resilience Engineering Research Center, School of Engineering, The University of Tokyo, 7-3-1 Hongo, Bunkyo-ku, Tokyo 113-8656, Japan

HIGHLIGHTS

- A direct solver of static liquid bridge via minimization of interfacial energy is developed.
- A model of liquid bridge force is proposed for sphere-sphere and sphere-plane configurations.
- The present model is applicable to asymmetric cases of unequal sphere radii and contact angles.
- The model is validated against the direct solution in various test problems.

ARTICLE INFO

Article history:
Received 14 December 2017
Received in revised form 16 February 2018
Accepted 18 February 2018
Available online 20 February 2018

Keywords:
Liquid bridge
Surface tension
Capillary force
Contact angle

ABSTRACT

The modeling of wet granular materials is an important research topic in chemical engineering. This study focuses on the numerical model for the capillary liquid bridge force in sphere-sphere and sphere-plane configurations, which is an indispensable ingredient of wet particle simulations. The first part of this study describes a direct approach via optimization of the interfacial energy of the liquid bridge system. The results, referred to as the optimal solutions, can be used as reference values for the exact solutions of static liquid bridges. In the second part, a force model is presented based on a toroidal approximation of the liquid bridge profile. Particularly, its advantage resides in the generality, which is applicable to a wide range of liquid volumes, contact angles and radius ratios. Predictions by the proposed model are validated against experimental data and optimal solution, from which good agreements are obtained. Numerical tests indicate that the relative error by the proposed model is generally below 10% within a wide range of contact angles and liquid volumes, showing its satisfactory accuracy for calculating the capillary force. It is expected that the present model will be useful for practical numerical analysis of wet granular materials.

1. Introduction

Wet granular materials are widely encountered in chemical engineering. When the liquid amount is relatively low, pendular liquid bridges are found between particles inside the solid layer (Mitarai and Nori, 2006). Usually, the liquid bridge force arising from capillary pressure and tensile force tends to induce strong cohesions that bind the particles together. The impact of liquid bridges on the flow behaviors of wet granular materials is very significant, by which not only the mechanical properties but also dynamic responses are drastically changed from their dry states (Jarray et al., 2017; Tegzes et al., 2003). Engineering examples of productive processes involving the liquid bridge include agglomeration (Tsunazawa et al., 2016), compaction (Mitchell et al., 2017), fluidization (Girardi et al., 2016; Tang et al., 2017), mixing (Liu et al., 2013; Remy et al., 2012), and multiphase dispersion (Georgiev et al., 2018). Therefore, an accurate model for the liquid bridge force is both scientifically fundamental and practically important in order to understand and optimize the operational conditions of wet particle processing. Especially, the modeling of capillary bridge can facilitate the application of engineering methods based on numerical analysis, such as the dynamic particle simulation using the discrete element method (DEM) (Cundall and Strack, 1979), which is able to reveal the particle behaviors at a grain level.

From a physical point of view, it is usually instructive to consider liquid bridges in two different regimes, namely the constant pressure case and the constant volume case, respectively (de Boer and de Boer, 2007; Israelachvili, 2010; Rabinovich et al., 2005). The constant pressure case is typically associated with the liquid-vapor

* Corresponding authors.
E-mail addresses: song@dem.t.u-tokyo.ac.jp (X. Sun), mikio_sakai@n.t.u-tokyo.ac.jp (M. Sakai).

https://doi.org/10.1016/j.ces.2018.02.034
0009-2509/

bridges formed during capillary condensation. By assuming a state of thermodynamic equilibrium, the capillary pressure can be related to the relative humidity according to the famous Kelvin equation, see e.g. (Israelachvili, 2010). In other words, a constant pressure liquid bridge may gain or lose mass from surrounding vapor to maintain the curvature of its meniscus. The constant pressure regime may be important for microscopic particles and volatile liquids, see e.g. (Dörmann and Schmid, 2014; Yang et al., 2010). On the other hand, the alternative case assumes a constant volume during bridge deformation, which may correspond to an involatile liquid or a sufficiently rapid process that evaporation/condensation can be neglected. Unlike the constant pressure case, the pressure cannot be determined directly in the constant volume regime, which leads to particular difficulties in calculating the capillary force. Therefore, in the present study, we mainly focus on liquid bridges subject to the constant volume condition.

Consider a static liquid bridge between two spherical particles. We assume that the separation distance, liquid volume and contact angles are known as fixed values. In fact, the liquid bridge has an interface of constant mean curvature as described by the Laplace-Young equation. Therefore, by integrating the differential equation with proper conditions meeting the liquid volume and contact angles, the direct solution of the bridge profile can be obtained. This method is commonly used in many past studies, see e.g. (Dörmann and Schmid, 2014; Lambert and Delchambre, 2005; Lian et al., 1993; Mikami et al., 1998; Soulié et al., 2006; Wang et al., 2016; Willett et al., 2000; Zhou and Ma, 2016). An alternative approach to directly solve the liquid bridge problem consists in optimizing the bridge profile targeting the one associated with minimal interfacial energy, of which the result is equivalent to the previous method. The famous Surface Evolver software (Brakke, 1992) has been used to obtain such "optimal solutions" in an interactive manner by Ardito et al. (2014); Broesch and Frechette (2012); Farmer and Bird (2015); Lambert et al. (2008). In recent years, with the increasing computational power, it also becomes possible to resolve the liquid bridge by direct numerical simulation (DNS) of multiphase flow systems, see e.g. (Darabi et al., 2010; Kan et al., 2015; Sun and Sakai, 2016; Washino et al., 2013).

Analytical models have also been proposed by different authors to write the liquid bridge forces in closed forms, usually as a function of the particle size, separation distance, contact angle and liquid volume. A very compact equation is given in Israelachvili (2010) and a similar one can be found in Rabinovich et al. (2005). Due to their simplicity, those models are used in some studies, see e.g. (Balakin et al., 2015; Liu et al., 2011; Tsunazawa et al., 2016). Their performance is, however, limited by the relatively small range of validity such as assumption of small volumes, near-zero contact angles and close distances (for example, our previous benchmark (Sun and Sakai, 2016) shows that the Rabinovich model is most accurate for liquid-solid ratio below 4% and contact angle smaller than 15°). Some other authors develop their model equations of liquid bridge force through curve fitting to data points obtained as exact solutions, see e.g. (Mikami et al., 1998; Soulié et al., 2006; Willett et al., 2000). As a matter of course, this approach is restricted by the availability of their original data, beyond which the model may not be extended successfully. Besides, the regression equations may have a considerably elaborate form that is difficult to find for general conditions (an example is that of Willett et al. (2000)). A comparative study of the above models can be found in Gladkyy and Schwarze (2014).

Geometric approximation is a useful method by which the liquid bridge problem can be simplified to facilitate the derivation of model equations. The toroidal approximation, since its first appearance in Fisher (1926), has been employed to model liquid bridges. In this approach, the meridional shape of the axisymmetric liquid bridge is fitted to a circle, from which further geometric relationship may be derived to construct an approximate solution of the liquid bridge. The model by Huppmann and Riegger (1975) which extends the work of Heady and Cahn (1970) seems to be a first model of the liquid bridge force based on the methodology of toroidal approximation. According to our previous study (Sun and Sakai, 2016), the Huppmann-Riegger model is able to predict the liquid bridge force with reasonable accuracy and generality. Several recent studies may be considered as refinements of the toroidal approximation method to account for asymmetry in particle sizes and contact angles. The model of Chen et al. (2011) takes the particle radius ratio into consideration, but the contact angles are required to be equal. Similarly, non-uniform particles are treated by the model of Harireche et al. (2013), whereas the contact angle is fixed to zero. Payam and Fathipour (2011) presents a model allowing for varying radius ratio and contact angle. However, their model equations are in a highly complicated form and seems to be insufficient in some key procedures to calculate the resultant force, which makes the applicability of their model somewhat unclear. Therefore, it is recognized that there is still some imperfection concerning the accuracy and generality of liquid bridge force modeling when applied to arbitrary liquid volumes, size ratios and contact angles. For similar reasons, the force model for a liquid bridge between a particle and a flat has not been thoroughly established yet.

The objective of the present study is to develop accurate and general models for the capillary force by the liquid bridge in sphere-sphere and sphere-plane configurations. A plausible application of the present model is the recent discrete particle simulations (see e.g. (Shigeto and Sakai, 2013; Sun et al., 2014; Sun and Sakai, 2015)), which must be enriched by an accurate model of inter-particle capillary force to treat wet granular materials.

In the first part of this paper, a direct solver in the axisymmetric coordinate is contributed, which is based on the energetic description of liquid bridges in equilibrium. The bridge interface is discretized by a series of linear elements with endpoints constrained on solid surfaces. The final shape of the meniscus is obtained by seeking the state associated with the minimum interfacial energy, from which the liquid bridge force is calculated. This approach has a unique advantage in that it can automatically reject the ambiguous metastable (but physically unstable) solutions by directly integrating the Laplace-Young equation (Lian et al., 1993; Lian and Seville, 2016) while keeping results that are physically admissible. It is thus more straightforward to calculate liquid bridges by using this method. This specialized solver is also more efficient and suitable for axisymmetric systems than general multiphase DNS solvers (Sun and Sakai, 2016). The optimal solutions given by this direct approach are very accurate, which can be used as reference values for liquid bridge problems.

The second part of this study develops a liquid bridge force model which uses the technique of toroidal approximation. The embracing angle, namely the angle subtending the contact ring on the solid surface, is given implicitly by a function related to the liquid volume. By solving the implicit function, the geometry of the liquid bridge is determined, from which the force can be calculated consequently. Model expressions and numerical algorithm are detailed in the paper. Various tests are conducted to validate the model against the experimental data and optimal solution. The present model is thought to be advantageous in the following aspects. Firstly, it is applicable to a wide range of liquid volumes and contact angles that may varies from small-volume (liquid-solid volume ratio $\sim 10^{-4}$) to large-volume (liquid-solid volume ratio ~ 0.2) regimes and from hydrophilic (perfect wetting, contact angle of 0°) to hydrophobic (tested to 150°) contact angles. Secondly, it is able to handle asymmetric liquid bridges where the particle radii and contact angles may differ. In fact, special treatments

are provided to assure that the liquid bridge with high asymmetry (e.g. between two surfaces with different wettability) can be calculated with satisfactory accuracy. To the authors' best knowledge, this seem to be the first one capable of modeling such liquid bridges. Lastly, it also includes a variant for the liquid bridge between a spherical particle and a flat wall, which performs as well as the original version. A number of validation tests have been performed by comparing the proposed model with experimental data and optimal solution to examine its accuracy.

In addition, some Matlab programs implementing the direct solver and the force model described in the paper are provided as Supplementary materials to help the readers to understand and compute the liquid bridges.

2. Problem description

2.1. Liquid bridge geometry

An axisymmetric liquid bridge connecting two spheres is shown in Fig. 1. The spheres have radii equal to R_1 and R_2, respectively, and their surfaces are separated by distance H. The curved bold line shows the interface of the capillary bridge, of which the total volume is V and the contact angles are θ_1 and θ_2 on the two ends. The two embracing angles, α_1 and α_2, are geometrical parameters defining the positions of contact rings b_1 and b_2 on solid surfaces. Similarly, Fig. 2 shows the sphere-plane case where the right sphere is replaced by a solid plane. In this case, the right embracing angle α_2 is undefined; instead, the finite contact radius b_2 still exists for the wall side.

If the gravity effect is insignificant, the static liquid bridge must have a constant-curvature surface. For an axisymmetric bridge, the curvature κ is composed of two principle curvature radii, namely the "inner" radius ρ_{in} of the radial direction and the "outer" radius ρ_{out} of the meridian (see Fig. 1). The interface curvature κ is thus given by Israelachvili (2010)

$$\kappa = \frac{1}{\rho_{in}} - \frac{1}{\rho_{out}} \tag{1}$$

It is noted that the inner curvature radius ρ_{in} is always positive, while the outer curvature radius ρ_{out} may be positive or negative according to the convexity of the bridge interface. In this study, ρ_{out} is designated to have positive sign for a concave bridge.

2.2. Liquid bridge force

Let the surface tension be σ, the Laplace pressure inside the bridge is given by Israelachvili (2010)

$$p = \sigma\kappa \tag{2}$$

The liquid bridge force can be obtained by integrating the Laplace pressure over the contact area and the surface tension along the contact ring for either of the two spheres (or the wall) (Huppmann and Riegger, 1975):

$$F = -p\pi R^2 \sin^2\alpha + 2\sigma\pi R \sin\alpha \sin(\alpha+\theta) \tag{3}$$

The second term arising from the tension is always attractive because of the the tensile capillary force. On the other hand, the first pressure term may be attractive ($p < 0$) or repulsive ($p > 0$). In this study, we follow the specification that the attractive force has plus sign and the repulsive force has minus sign.

In fact, the force can be calculated for any cross-sectional plane along the bridge axis, since it is in mechanical equilibrium. For instance, if the liquid bridge has a "neck" or "waist" where the minimal or maximal radius is ρ, the force can be evaluated therein as (Hotta et al., 1974)

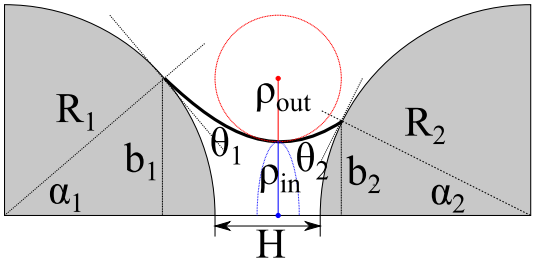

Fig. 1. Axisymmetric liquid bridge between two spheres. The meniscus is indicated by the bold line, of which the radial and meridional curvature radii are ρ_{in} and ρ_{out}, respectively. The embracing angles α_1 and α_2 correspond to the contact rings b_1 and b_2 on the two solid surfaces.

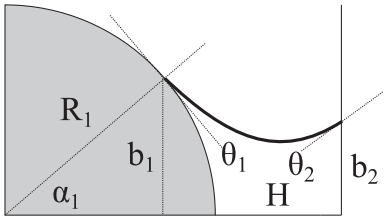

Fig. 2. Axisymmetric liquid bridge between sphere and plane. Notations are similar to the previous sphere-sphere case, except that the right-hand contact ring b_2 is planar and thus a subtending angle cannot be defined.

$$F = -p\pi\rho^2 + 2\sigma\pi\rho \tag{4}$$

The definitions (3) and (4) can be used to calculate the force once the shape of the liquid bridge is known.

2.3. Analytical models

Provided that the sphere radii R_1 and R_2, separation H, contact angles θ_1 and θ_2, and total liquid volume V_L are given, a typical problem posed for the liquid bridge system is to find its geometry and force. Therefore, the liquid bridge force F is considered to be a function of the following form:

$$F = F(R_1, R_2, H, \theta_1, \theta_2, V_L) \tag{5}$$

By making necessary simplifications to the liquid bridge problem, analytical equations for liquid bridge force have been derived, which may reside in assuming zero contact angles/separations, small liquid volumes (Israelachvili, 2010), or approximation by circular shapes (Heady and Cahn, 1970). A useful explicit equation is that given in Rabinovich et al. (2005):

$$F = \frac{2\pi R\sigma\cos\theta}{1 + H/2d} \tag{6}$$

where

$$d = \frac{H}{2}\cdot\left(-1 + \sqrt{1 + \frac{2V_L}{\pi RH^2}}\right) \tag{7}$$

It is known that the Rabinovich equation applies to liquid bridges with small volumes or small contact angles (Lambert et al., 2008; Sun and Sakai, 2016). Another import model is derived by Huppmann and Riegger (1975) for particle sintering processes:

$$F = p\pi R^2 \sin^2\alpha + 2\pi R\sigma \sin\alpha \sin(\alpha+\theta) \tag{8}$$

Herein, the pressure jump p is calculated from curvature κ as Eq. (2). The Huppmann-Riegger model adopts the toroidal approximation of the bridge profile, which indicates the following relationships between the embracing angle α and the inner/outer principle curvature radius:

$$\rho_{in} = R\sin\alpha - \rho_{out}(1-\sin(\alpha+\theta))$$
$$\rho_{out} = \frac{R(1-\cos\alpha)+H/2}{\cos(\alpha+\theta)} \tag{9}$$

The embracing angle α is further related to the total liquid volume by

$$V_L = 2\pi(\cos(\alpha+\theta)-(\pi/2-\alpha-\theta))(\rho_{out}^3+\rho_{in}\rho_{out}^2) + \pi\rho_{in}^2\rho_{out}\cos(\alpha+\theta) \tag{10}$$

One must solve the implicit volume equation to obtain the embracing angle which may be then substituted into the force equation (8). In spite of the increased complexity due to its implicitness, the Huppmann-Riegger model is applicable to a wider range of liquid bridge conditions (Sun and Sakai, 2016).

It is noted that both the Rabinovich model and the Huppmann-Riegger model are derived for equal spheres. For unequal spheres, effective equations based on the Derjaguin approximation (Israelachvili, 2010) must be used to adapt those models. The effective radius and contact angle are computed as follows:

$$\frac{1}{R_{eff}} = \begin{cases} \frac{1}{2}\left(\frac{1}{R_1}+\frac{1}{R_2}\right) & \text{sphere}-\text{sphere} \\ \frac{1}{2R_1} & \text{sphere}-\text{plane} \end{cases}$$
$$\cos\theta_{eff} = \frac{1}{2}(\cos\theta_1+\cos\theta_2) \tag{11}$$

where the individual radii and contact angles are defined in Fig. 1.

3. Optimal solution

In this section, we describe a numerical approach based on optimization of interfacial energy to obtain the reference solution of axisymmetric liquid bridges. The numerical solutions obtained by this approach will be referred to as "optimal solution" hereinafter.

3.1. Numerical method

As shown in Fig. 3, the meniscus is discretized by N linear segments with $(N+1)$ nodes labeled from P_0 to P_N, whose axial and radial positions are $\{x_i, r_i\}$ $(i = 0, 1, \ldots, N)$, respectively. Fig. 3 also illustrates the X-R coordinate whose origin is at the center of the left sphere. We minimize the following form of free energy W of the liquid bridge system to obtain a valid static solution (Lambert et al., 2008):

$$\min_{\{x_i,r_i\}} W = \sigma(S_{GL} - S_1\cos\theta_1 - S_2\cos\theta_2) \tag{12}$$

Herein, S_{GL} is the area of the lateral bridge surface separating the gas-liquid phase. It is given by a direct quadrature by the midpoint rule summing over all revolved elements:

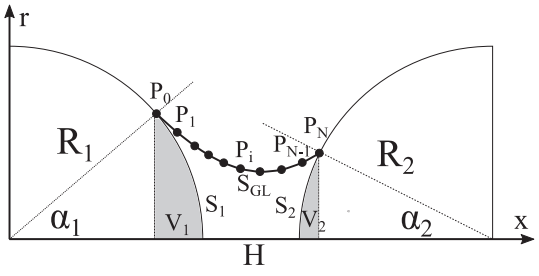

Fig. 3. Discretized bridge interface by linear elements. The meniscus is modeled by N segments with $(N+1)$ points $P_0, P_1, \ldots, P_N$. The two endpoints (P_0 and P_N) must lie on the sphere surface. With this discretization, the gas-liquid surface S_{GL} is given by revolution around the x-axis, and the solid-liquid surfaces (S_1 and S_2) correspond to the spherical caps beneath the contact points. The liquid volume is equal to subtracting the immersed volumes (V_1 and V_2) from the total volume of revolution.

$$S_{GL} = 2\pi\sum_{i=1}^{N}\frac{(r_i+r_{i-1})}{2}\cdot l_i$$
$$l_i = \sqrt{(x_i-x_{i-1})^2+(r_i-r_{i-1})^2} \tag{13}$$

The contact areas S_1 and S_2 are the areas of sphere caps immersed by the liquid bridge, which can be obtained from the embracing angles α_1 and α_2 determined by the two endpoints:

$$S_1 = 2\pi R_1^2(1-\cos\alpha_1)$$
$$S_2 = 2\pi R_2^2(1-\cos\alpha_2) \tag{14}$$

$$\alpha_1 = \arctan\left(\frac{r_0}{x_0}\right)$$
$$\alpha_2 = \arctan\left(\frac{r_N}{R_1+H+R_2-x_N}\right) \tag{15}$$

The solution procedure is thus achieved by optimization of the nonlinear target function (12) by adjusting the nodal positions $\{x_i, r_i\}$ $(i = 0, 1, \ldots, N)$ subject to three constraints as follows.

(a) Constraint of liquid volume.

The volume V surrounded by the lateral interface and two sphere caps must be equal to the original liquid volume V_L, i.e.

$$1 - V(\{x_i, r_i\})/V_L = 0 \tag{16}$$

The volume V is computed by

$$V = V_{rot} - V_1 - V_2 \tag{17}$$

in which the volume of the body of rotation is integrated by summing the slices of each element:

$$V_{rot} = \pi\sum_{i=1}^{N}\left(\frac{r_{i-1}+r_i}{2}\right)^2(x_i-x_{i-1}) \tag{18}$$

The volumes V_1 and V_2 are associated with the immersed sphere caps (i.e. the shaded parts in Fig. 3).

$$V_1 = \frac{\pi}{3}R_1^3(2-3\cos\alpha_1+\cos^3\alpha_1)$$
$$V_2 = \frac{\pi}{3}R_2^3(2-3\cos\alpha_2+\cos^3\alpha_2) \tag{19}$$

(b) Constraint of contact points.

The two endpoints of the discretized bridge interface, P_0 and P_N, must lie on the sphere surfaces, i.e.

$$\sqrt{x_0^2+r_0^2} = R_1$$
$$\sqrt{(x_N-(R_1+H+R_2))^2+r_N^2} = R_2 \tag{20}$$

This constraint guarantees that the embracing angles can be computed directly from the positions of corresponding endpoints.

(c) Constraint of equidistant node positions.

Additionally, we require that all nodes are equally distributed along the axial direction:

$$x_i - x_0 = \frac{x_N-x_0}{N}i \tag{21}$$

Note that this is a linear constraint. Although this condition is not essential, it seems to help improve the convergence based on our numerical tests.

The optimization problem can be treated with any modern general-purpose optimizers supporting nonlinear constraints. In this study, a Matlab code is developed and the FMINCON function

from the Optimization Toolbox is employed using the sequential quadratic programming (SQP) algorithm[1]. The numerical tolerance is set to 10^{-8} to ensure that the solution converges maturely. As a first guess, the bridge shape is initialized as a straight cylinder with the same original liquid volume.

As for the sphere-plane case, it is not recommended to set extremely large size ratio $R_2/R_1 >> 1$ to model the flat, which may slow down the convergence and cause deterioration of accuracy. Direct modeling of the plane is always preferable. The present model can be adapted to the sphere-plane geometry straightforwardly with a few modifications. In particular, the right endpoint should have its x-coordinate constrained on the wall, the immersed volume V_2 vanishes to zero, and the contact area S_2 collapses to a flat circle thereby. Details can be found in the source code attached.

3.2. Force calculation

When it comes to the calculation of capillary bridge force, there are two approaches, namely the energetic method and the geometric method (Lambert et al., 2008). In the energetic method, the force is obtained by differentiating the free energy W with respect to the separation H, which could be accurately approximated by the following finite centered difference form:

$$F = \frac{dW}{dH} \approx \left.\frac{W(H+\Delta H) - W(H-\Delta H)}{2\Delta H}\right|_{R_1,R_2,\theta_1,\theta_2,V_L} \tag{22}$$

In the geometric method, the Laplace pressure p and the embracing angle α are first computed from the bridge geometry, and then they can be used together with the definition (3) to work out the force. In principle, the two approaches are equivalent, and they are both applicable to the present model. It is noted that, if the energetic method is employed, the optimal solution must be calculated twice in order to carry out the central difference. On the other hand, in the geometric method, the solution is calculated once, from which the Laplace pressure can be obtained directly as

$$p = \lambda / V_L \tag{23}$$

where λ is the Lagrange multiplier associated with the volumetric constraint, which is available from the optimizer. As a matter of course, one may also calculate the curvature via the nodal positions and use Eq. (2) to get the pressure, which yields the same results as the current approach.

In this study, we use $N = 50$ elements (51 nodes) for discretization of the axisymmetric interface. This resolution seems to work properly of most cases according to our tests. Results of a refinement test is presented in Table 1 with $R = 1$, $\theta = 0$, $H = 0$ and $V = 0.001$. Further increasing the number of elements does not improve the result of force calculation significantly.

4. Force model

In this section, we present the modeling of liquid bridge based on the toroidal approximation. The axisymmetric sphere-sphere case and sphere-plane case will be considered, where the sphere radii and contact angles are not necessarily equal.

4.1. Sphere-sphere case

Fig. 4 shows the sphere-sphere case, where the bridge interface is approximated by a circular arc whose endpoints are on the sphere surfaces. At their intersections, the tangents of the sphere and the interface subtend the contact angles θ_1 and θ_2, respectively.

[1] See the Matlab document: https://www.mathworks.com/help/optim/ug/fmincon.html.

Table 1
Influence of element refinement on force calculation.

	$N = 25$	$N = 50$	$N = 100$
$F/\sigma R$	5.796	5.829	5.843

*Radius $R = 1$, contact angle $\theta = 0$, separation $H = 0$, and volume $V = 0.001$.

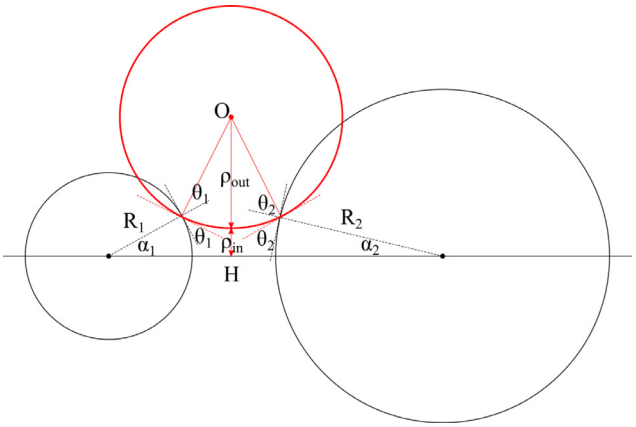

Fig. 4. Toroidal approximation of a liquid bridge between two spheres. The meniscus is represented by the red circle O. The two principle curvatures (ρ_{in} and ρ_{out}) are measured at the neck of the bridge.

The radius of the circular interface is denoted by ρ_{out}, and the transverse radius of the bridge is ρ_{in} at the "neck" or "waist" position. In this problem, the known values are the sphere radii R_1 and R_2, the separation H, the contact angles θ_1 and θ_2, and the liquid volume V_L, while the unknowns are the embracing angles α_1 and α_2 and the curvature radii ρ_{out} and ρ_{in}. We will derive equations of those geometrical parameters and reduce them to functions of the left embracing angles α_1 for convenience.

Based on the simple geometrical relationship indicated in Fig. 4, the outer curvature radius can be expressed by the embracing angles as follows:

$$\rho_{out} = \frac{R_1(1-\cos\alpha_1) + R_2(1-\cos\alpha_2) + H}{\cos(\alpha_1+\theta_1) + \cos(\alpha_2+\theta_2)} \tag{24}$$

The inner curvature radius is related to the left embracing angle by

$$\rho_{in} = R_1 \sin\alpha_1 - \rho_{out}(1 - \sin(\alpha_1+\theta_1)) \tag{25}$$

Swapping the particle labels, we have a similar equation for the right embracing angle:

$$\rho_{in} = R_2 \sin\alpha_2 - \rho_{out}(1 - \sin(\alpha_2+\theta_2)) \tag{26}$$

Although this equation is not used in actual computation, by equating it with Eq. (25), the following relationship between the two embracing angles is obtained:

$$-\frac{R_1\sin\alpha_1 - R_2\sin\alpha_2}{\sin(\alpha_1+\theta_1) - \sin(\alpha_2+\theta_2)} = \frac{R_1(1-\cos\alpha_1) + R_2(1-\cos\alpha_2) + H}{\cos(\alpha_1+\theta_1) + \cos(\alpha_2+\theta_2)} \tag{27}$$

After some algebra applying the sum-to-product identities of trigonometric functions, we find a result for the embracing angles:

$$\tan(\alpha_2/2) = \frac{R_1 A + AH/2 + CH/2}{R_2 + H/2 - AC(R_1 + R_2 + H/2)} \quad \text{with } A = \tan(\alpha_1/2),\ C = \tan((\theta_1-\theta_2)/2) \tag{28}$$

Specifically, if $\theta_1 = \theta_2$, we have $C = 0$ and a simplified equation that writes

$$\tan(\alpha_2/2) = \frac{R_1 + H/2}{R_2 + H/2}\tan(\alpha_1/2) \tag{29}$$

This is the relationship for equal contact angles similar to that derived by Chen et al. (2011).

As shown above, we are able to compute the relevant geometrical parameters including the outer curvature radius ρ_{out} (Eq. (24)), the inner curvature radius ρ_{in} (Eq. (25)) and the right embracing angle α_2 (Eq. (28)) as functions of the left embracing angle α_1. In order to finally close this system, we resort to the conservation of the original liquid volume V_L. The volume of the body by revolving the circular surface is

$$\begin{aligned} V_{rot} = {} & \pi\rho_{out}((\rho_{out}+\rho_{in})^2 + \rho_{out}^2)(\cos\phi_1 + \cos\phi_2) \\ & + \pi\rho_{out}^2(\rho_{out}+\rho_{in})(\phi_1 + \phi_2 - \pi) \\ & - \pi\rho_{out}^2(\rho_{out}+\rho_{in})(\sin\phi_1\cos\phi_1 + \sin\phi_2\cos\phi_2) \\ & - \frac{\pi}{3}\rho_{out}^3(\cos^3\phi_1 + \cos^3\phi_2) \end{aligned} \tag{30}$$

$$\phi_1 = \alpha_1 + \theta_1$$

$$\phi_2 = \alpha_2 + \theta_2$$

Therefore, the total liquid volume must satisfy

$$V_L = V(\alpha_1, \alpha_2, \rho_{out}, \rho_{in}) = V_{rot} - V_1 - V_2 \tag{31}$$

where V_1 and V_2 are the volumes of the spherical caps submerged in the liquid given by Eq. (19). Apparently, this equation is an implicit function of the left embracing angle. Our volume relation (31) contains all terms from the Huppmann-Riegger model (10) if the liquid bridge is symmetric. The equation of Chen et al. (2011) is also a special case of Eq. (31) with equal contact angles.

4.2. Sphere-plane case

The sphere-plane case is illustrated in Fig. 5. Only minor changes are required for the model described in the previous section. Noticing that the right embracing angle α_2 and immersed volume V_2 vanishes, we simply enforce $R_2 = 0$ and $\alpha_2 = 0$ in this case. Eq. (28) is thus discarded, while the rest of the equations (outer radius (24), inner radius (25), and volume (31)) remain intact.

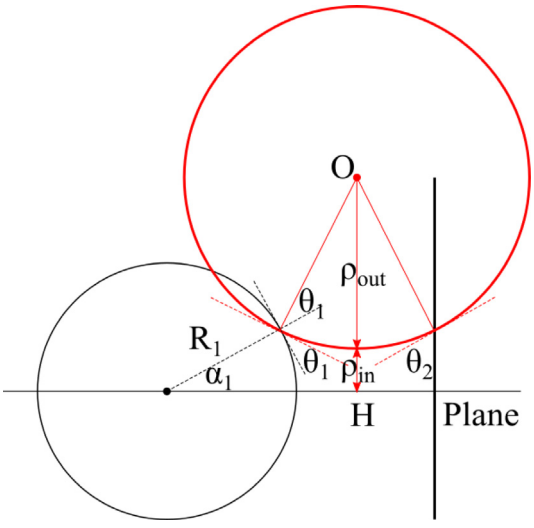

Fig. 5. Toroidal approximation of a liquid bridge between sphere and plane. Similar to the previous figure, but note that the right embracing angle is undefined for the flat.

4.3. Solution procedure

The following nonlinear equation indicated by the volume relationship (31) must be solved for the unknown embracing angle α_1:

$$g(\alpha_1) = V(\alpha_1)/V_L - 1 = 0 \tag{32}$$

In this study, the Newton's method is used for root-finding, owing to its fast rate of convergence (Press et al., 2007). In the Newton's method, it begins with some initial guess, and successively improves the solution until the original equation is satisfied. For the k-th cycle, it proceeds as

$$\alpha_1^{k+1} = \alpha_1^k - g(\alpha_1^k)/g'(\alpha_1^k) \tag{33}$$

Since the target function g represents the relative volume error, the error tolerance is determined by a relative volume error $|g| < 10^{-6}$ for convergence. Hence, the volume is conserved almost exactly.

The application of the Newton's method requires that the derivative g' should be calculated with respect to the embracing angle. However, the complicated form (30) implies that the analytical expression may not be convenient to use. Instead of the exact form, we use a finite difference (FD) to estimate the derivative:

$$g'(\alpha_1) \approx \frac{g(\alpha_1 + \Delta\alpha) - g(\alpha_1 - \Delta\alpha)}{2\Delta\alpha} \tag{34}$$

In this study, we have $\Delta\alpha = 10^{-6}$ as α_1 is the angle in radians. An alternative choice is to employ the automatic differentiation (AD) technique which has been widely used for computing gradients in various scientific applications (Neidinger, 2010). The advantage of AD is that it works without the exact expression and yields accurate results to the machine precision. In the context of the present study, the AD helps to improve the convergence under some marginal cases where the FD becomes unstable. In most cases, solutions using the FD and AD techniques are equivalent. The Matlab code in the Supplement material implements both methods.

A good initial guess of α_1 is critical for the convergence. In this study, we heuristically find the following condition (see derivation in Appendix A):

$$\alpha_{guess} = \sqrt{\frac{-\frac{H}{R_1} + \sqrt{\frac{H^2}{R_1^2} + C\frac{V_L}{\pi R_1^3}}}{C/2}}$$

$$C = \begin{cases} 1 + R_1/R_2 & \text{sphere} - \text{sphere} \\ 1 & \text{sphere} - \text{wall} \end{cases} \tag{35}$$

Beginning with this initial guess, in general, the solver will converge to the desired accuracy (relative volume error smaller than 10^{-6}) in three iterations. Once the key parameter of left embracing angle is obtained, the other parameters can be calculated, and the bridge shape is determined consequently. In the next section, we explain the calculation of liquid bridge force along with its geometrical information.

4.4. Force calculation

For the liquid bridges shown in Fig. 4 (sphere-sphere) and Fig. 5 (sphere-plane), a "neck" or "waist" lives on the actual bridge profile corresponding to the inner curvature radius. The liquid bridge force is calculated at such an inflection apex by

$$\begin{aligned} F &= -p\pi\rho_{in}^2 + 2\pi\sigma\rho_{in} \\ &= \pi\sigma\rho_{in}(1 + \rho_{in}/\rho_{out}) \end{aligned} \tag{36}$$

in which the definition (2) of Laplace pressure is used. This approach is sometimes referred to as the "gorge" method (Hotta et al., 1974).

An exceptional case may be found as in Fig. 6 where the neck position falls inside the sphere. In fact, such liquid bridges physically exists under certain conditions (e.g. when the surface wettability differs to a large extent (Wang et al., 2013)). Therefore, we extend the method of force calculation to this special case for more generality. Notice that the center of the circular interface is at

$$x_c = R_1 \cos\alpha_1 + \rho_{out}\cos(\alpha_1 + \theta_1) \tag{37}$$

which is also equal to the x-coordinate of the apex. Therefore, the bridge profile have a neck point if

$$R_1 \cos\alpha_1 \leqslant x_c \leqslant R_1 + H + R_2(1 - \cos\alpha_2) \tag{38}$$

If this is not satisfied, then there will be no neck point on the actual interface, which means that the gorge formula (36) may be invalid for using the improper curvature ρ_{in}. Rather, the inner curvature is estimated by using the following equation:

$$\begin{aligned} \bar{\rho}_{in} &= \frac{1}{2}(\rho_1 + \rho_2) \\ \rho_1 &= \frac{b_1}{\sin(\alpha_1 + \theta_1)}, \rho_2 = \frac{b_2}{\sin(\alpha_2 + \theta_2)} \end{aligned} \tag{39}$$

where b_1 and b_2 are the radii of contact rings on solids:

$$\begin{aligned} b_1 &= R_1 \sin\alpha_1 \\ b_2 &= b_1 + \rho_{out}\sin(\alpha_1 + \theta_1) - \rho_{out}\sin(\alpha_2 + \theta_2) \end{aligned} \tag{40}$$

Replacing ρ_{in} with the corrected value $\bar{\rho}_{in}$ in Eq. (1), the pressure p is determined by Eq. (2). Then we apply Eq. (3) to calculate the force for the two contact sites respectively:

$$\begin{aligned} F_1 &= -p\pi b_1^2 + 2\sigma\pi b_1 \sin(\alpha_1 + \theta_1) \\ F_2 &= -p\pi b_2^2 + 2\sigma\pi b_2 \sin(\alpha_2 + \theta_2) \end{aligned} \tag{41}$$

By taking their average, the capillary force of the liquid bridge without a neck point is

$$F = \frac{1}{2}(F_1 + F_2) \tag{42}$$

This treatment can be significant for capillary bridges with particular combination of contact angles. In addition, by fixing $R_2 = 0$ and $\alpha_2 = 0$ as done in Section 4.2, the equations provided above can be applied to the sphere-plane system without modification.

5. Validation by experimental data

In this section, the liquid bridge force model (Section 4) is validated against experimental data, and the optimal solution (Section 3) is also presented for comparison. In the past, several authors reported experiments of capillary bridge force between spheres by using atomic force microscope (AFM) type instruments or high-sensitivity microbalances. We will consider the results available from Rabinovich et al. (2005); Lambert et al. (2008) and Willett et al. (2000).

The first data set is taken from Rabinovich et al. (2005), which is obtained using an AFM for small (micrometric) liquid bridge systems. In their experiments, glass beads were glued to the AFM cantilever and the substrate, and mineral oil with a small contact angle was used to interconnect the particles. The three test cases are summarized in Table 2. From the table, the maximum liquid volume (regularized by the cube of particle radius) is smaller than 5.3×10^{-4}, which can be considered as a test for liquid bridges in the limit of small volumes. Fig. 7 plots the liquid bridge force against separation distance for each test case. The prediction by the present model is in good agreement with the experimental data and the optimal solutions.

The second data set is published by Lambert et al. (2008) whose authors discussed the limitation of Rabinovich's force model. They argued that the applicability of Rabinovich model is questionable for sufficiently large liquid volumes. Experiments of liquid bridges at a millimetric scale was carried out by using their specially

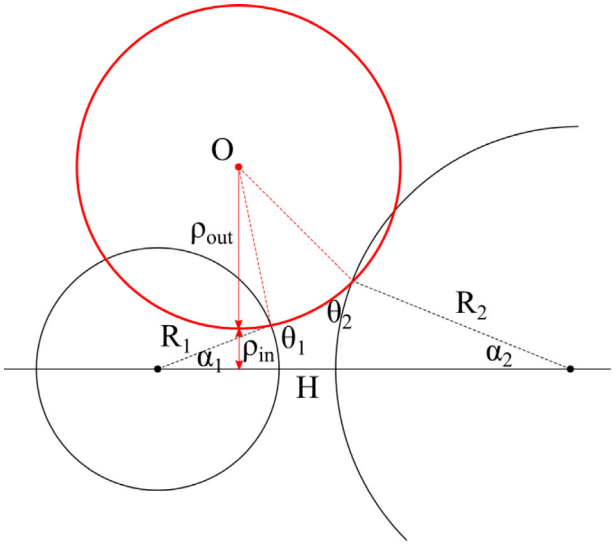

Fig. 6. Liquid bridge without real neck point. Due to asymmetries in radius and contact angle ($R_1 < R_2$ and $\theta_1 > \theta_2$ here), the center of toroidal approximation shifts and the neck point exists only imaginarily in the solid region.

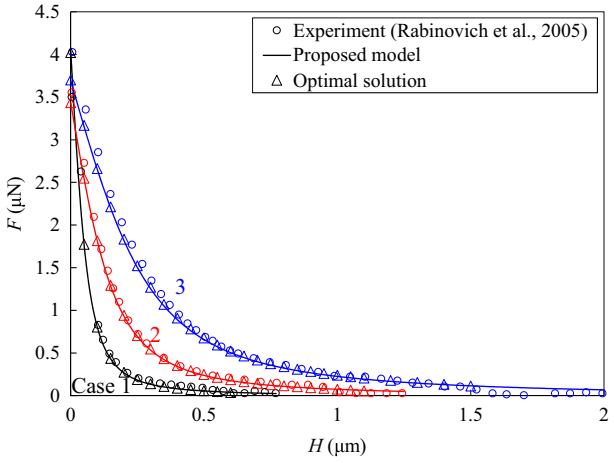

Fig. 7. Liquid bridge force of Rabinovich et al. (2005). The direct solutions by optimization are referred to as "optimal solution" in chart legends hereinafter. The three cases correspond to those listed in Table 2. Both the optimal solution and the model prediction are in good agreement with the experimental data.

Table 2
Liquid bridge parameters of Rabinovich et al. (2005).

	R_1 (μm)	R_2 (μm)	θ (degree)	σ (mN/m)	V (μm^3)
Case 1	19	35	10	27	0.2
Case 2		32.5		24	1.2
Case 3		27.5		28	3.6

Table 3
Liquid bridge parameters of Lambert et al. (2008).

	R_1 (mm)	R_2 (mm)	θ_1 (degree)	θ_2 (degree)	σ (mN/m)	V (mm^3)
Case 1	2	3.95	0	14.3	20.8	0.065
Case 2						1.4

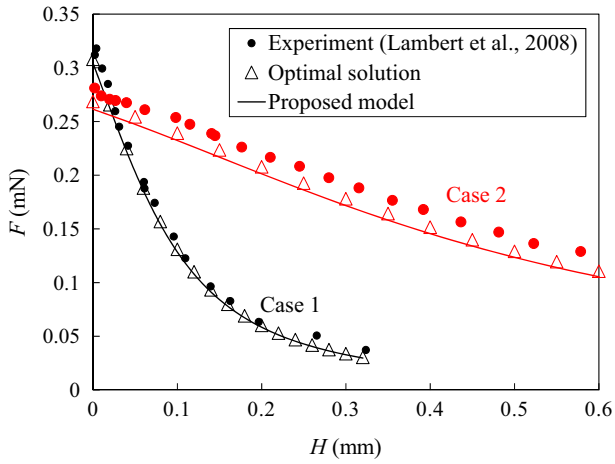

Fig. 8. Liquid bridge force of Lambert et al. (2008). The two cases are shown in Table 3 for different liquid volumes. The agreements with experimental data are visible.

designed device that worked in a similar way as AFM. Ruby and steel spheres were used together with silicone oil to form liquid bridges. According to the conditions in Table 3, Case 1 has a regularized volume of $V/R_1^3 = 8.1 \times 10^{-3}$; for Case 2, this value is 0.18. The results in Fig. 8 shows good agreement for the test data of both cases. In Case 2 the experimental data seems to be systematically larger than the numerical solutions, which is possibly due to errors in measurements as the model prediction matches the optimal solution. Therefore, the validity of the present model is proved for both small- and large-volume regimes of liquid bridge.

The third set of experimental data is retrieved from Willett et al. (2000), who examined the effect of sphere size ratio on liquid bridge force. In their experiments, the capillary force was measured by an accurate microbalance connected with sapphire particles. Almost perfect-wetting silicon fluid was added between the particles of different sizes or between the particle and a substrate. Among the four cases tabulated in Table 4, the left sphere is fixed and the right sphere is varied. In Cases 1–3, the ratios of radius are, respectively, 1:1, 3:2 and 2:1. Their results are plotted in Fig. 9(a–c). It is seen that for all sphere pairs with different radius ratios, the present model is in good agreement with the reference data. In Case 4, a sphere-plane geometry is considered, for which the results are shown in Fig. 9(d). Again, the agreement is remarkable. We have also tested the limiting case of the force model by setting a very large size ratio ($R_2/R_1 = 4\times10^2$) and obtained results (not shown) equivalent to those in Fig. 9(d). Therefore, it is shown that the present model can be readily applied to unequal sphere-sphere and sphere-wall problems.

6. Verification and comparison with other models

For the test of liquid bridge models, experimental validations are usually restricted by various conditions such as the material properties, accessibility of physical scales and errors/uncertainty of measurements, which increases the difficulty in obtaining a rich and accurate set of test data. In this regard, the direct optimal solutions may fill the void to verify and investigate the model extensively. Therefore, the objective of this section is to further test the performance of the current model within a wide range of parameters. In particular, the prediction of shape and force will be presented for liquid bridges in asymmetric configurations. The comparison with other analytical models are also shown to highlight the advantage of our model. For the sake of generality, results are rendered dimensionless in this section. The characteristic length scale is chosen as the sphere radius R. Since the choice is somewhat arbitrary, we will always use the smaller sphere radius (another choice is to use the reduced Derjaguin radius). Consequently, the liquid volume is normalized by a factor of R^3, and the force is normalized by σR.

6.1. Equal spheres

We begin the model test with identical spheres, for which the target is to show the effects of contact angles and liquid volumes. The volume was set to $V = 0.0209$ (approximately 0.5% sphere volume), and the contact angle was varied by $\theta = 15°$, 30°, 60° and 90°. The bridge profiles of 15° and 90° angles are shown in Fig. 10(a, b), respectively. In the figure, the red markers show the reference solution obtained by the optimization procedure and the blue circles are the results of the present model. Obviously, the shape is symmetric, and the meridional curve is concave for small contact angle (e.g. $\theta = 15°$) and becomes convex for large angle (e.g. $\theta = 90°$). This effect of contact angle is captured satisfactorily by the present model.

The liquid bridge forces are plotted as functions of the distance in Fig. 11, where the Rabinovich equation, the Huppmann-Riegger model and the present model are juxtaposed for comparison and the optimal solution is used as exact values. For contact angles below 60°, the force is attractive and decays with the separation distance; for a 90° neutral contact angle, the force is repulsive at close distance and reverses to be attractive at far distance. Relative errors in liquid bridge force (referring to the optimal solution) are 4.63%, 3.99%, 1.64%, and 1.37% in average for these four cases, respectively. Among the various models tested, the approach proposed in this study performs well achieving excellent agreements with the optimal solutions in all cases. Performance of the Huppmann-Riegger model is also reasonable, although the error becomes noticeable beyond a mediate distance. On the other hand,

Table 4
Liquid bridge parameters of Willett et al. (2000).

	R_1 (mm)	R_s (mm)	θ (degree)	σ (mN/m)	V (nL)
Case 1	2.381	2.381	0	20.6	13.6, 31.3, 74.2
Case 2		1.588			9.6, 13.2, 24.7, 59.3
Case 3		1.191			25.3, 61.8, 127.8
Case 4		– (wall)			162.4, 280.2

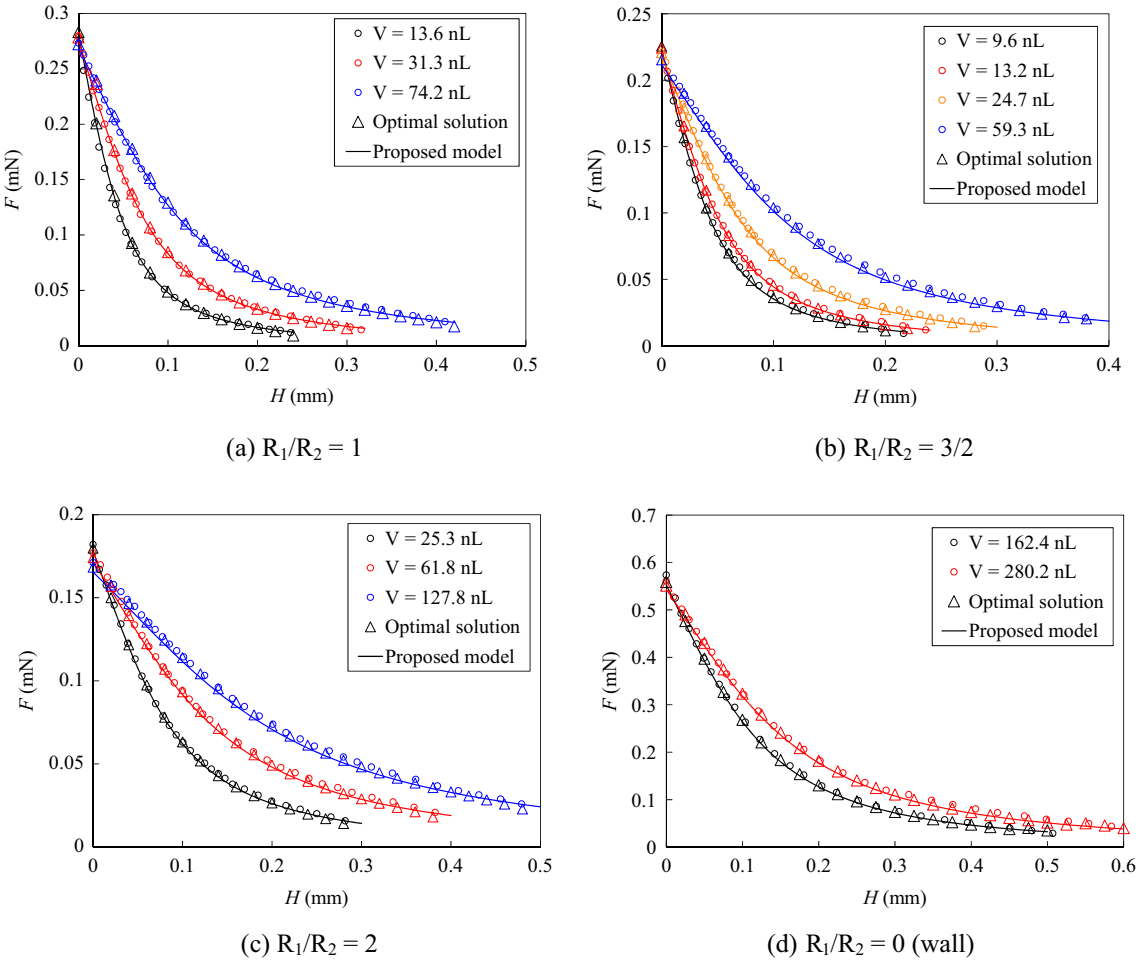

Fig. 9. Liquid bridge force of Willett et al. (2000). The panels correspond to four cases with different sphere size ratios (Table 4). For those configurations, the optimal solution (triangle marker) and the present model (solid line) are compared with experimental data (circle marker).

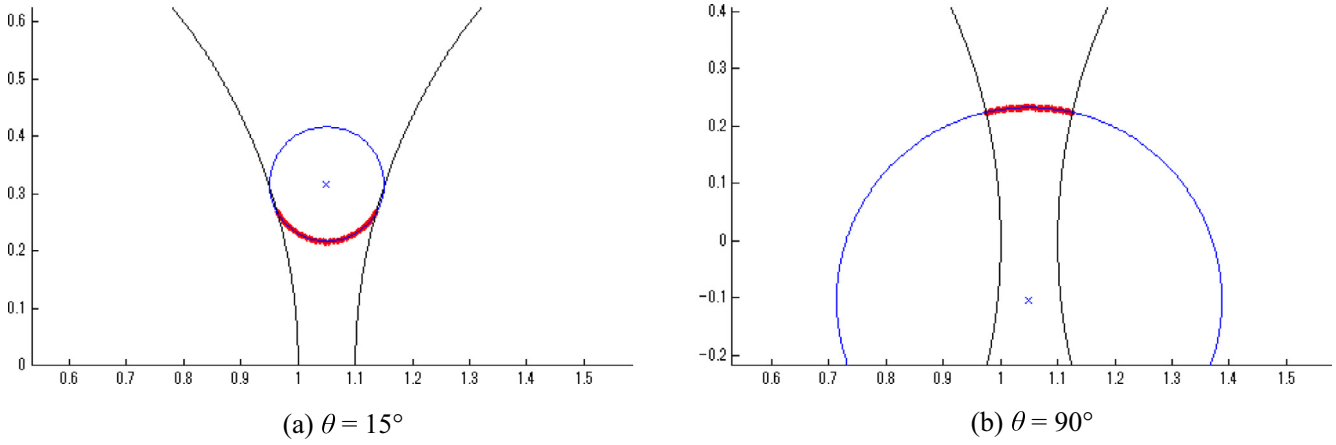

Fig. 10. Liquid bridge profiles between two equal spheres with $V = 0.0209$ and $H = 0.1$: (a) concave shape with $\theta = 15°$, (b) convex shape with $\theta = 90°$. The red markers show the optimal solutions, and the blue circle and cross symbol show the approximation by the present model.

the Rabinovich equation deviates from the reference solution as the contact angle increases. Especially, the force vanishes totally to zero in the 90° case, showing a severe loss of accuracy.

The present model has also been tested for another symmetric liquid bridge problem with volume $V = 0.838$ (approximately 20% sphere volume). As commented in our previous study (Sun and Sakai, 2016), two-body pendular liquid bridges are likely to coalesce into multibody funicular structures (Mitarai and Nori, 2006) under such a high liquid amount in actual porous solids. Therefore, this test is intended to examine the model performance at the volumetric upper limit. Fig. 12 shows the forces with contact angles ranging from 15° to 120°. The results of the present model

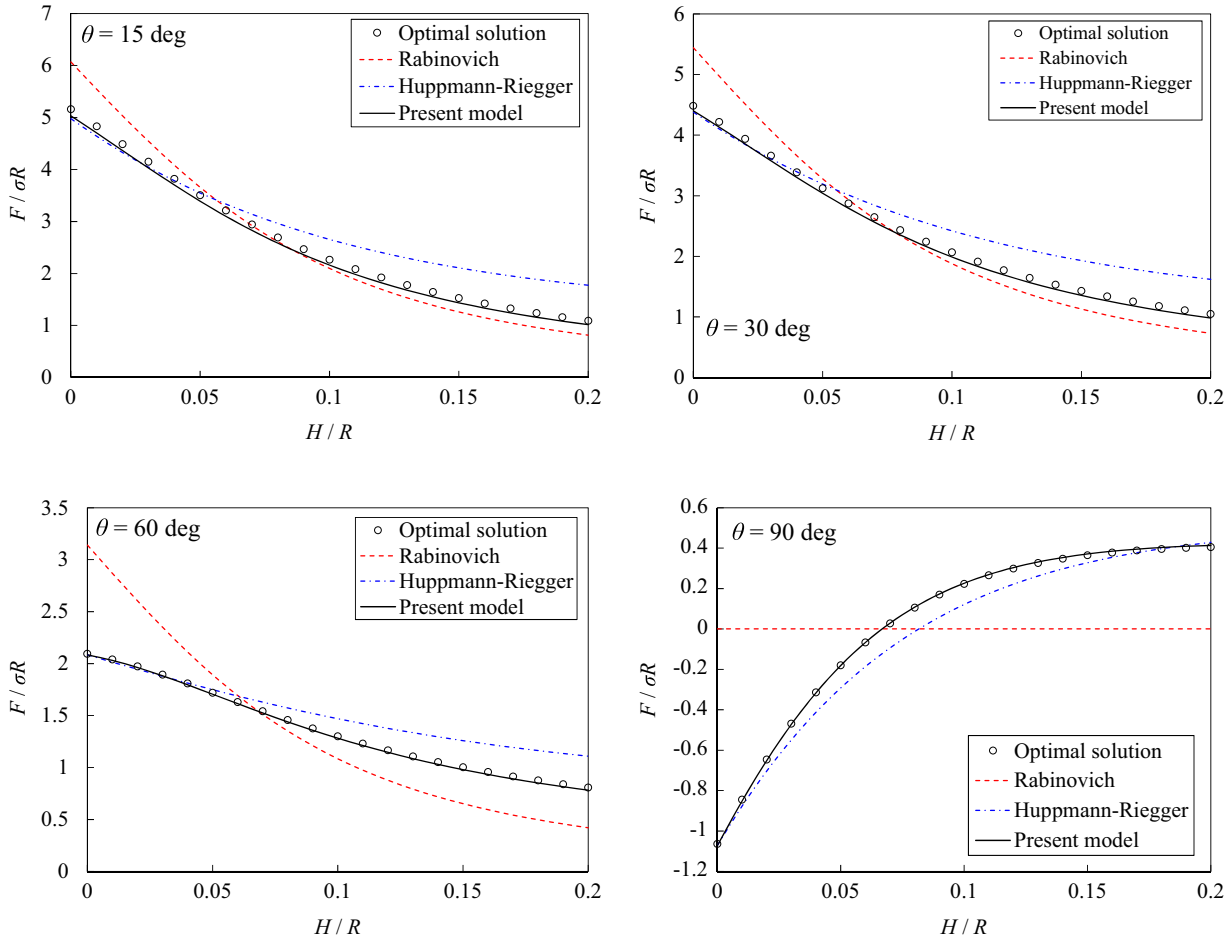

Fig. 11. Liquid bridge forces between equal spheres with $V = 0.0209$: (a) $\theta = 15°$, (b) 30°, (c) 60°, (d) 90°.

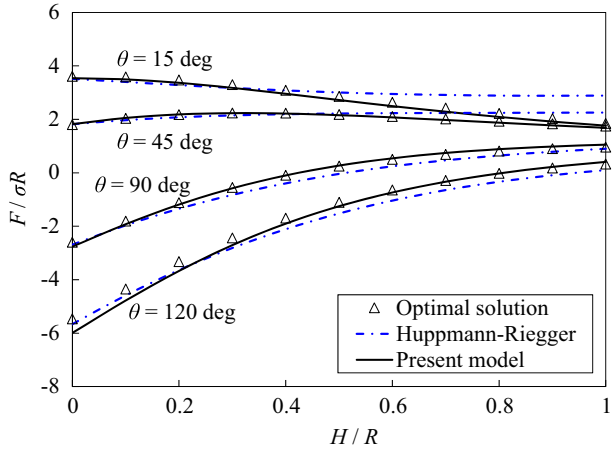

Fig. 12. Liquid bridge forces between equal spheres with $V = 0.838$.

agree reasonably with the optimal solution. The average relative error is 4.32% for 15°, 1.60% for 45°, 7.56% for 90° and 14.4% for 120°, respectively. It is noted that the visible error in 90° and 120° cases should be mainly ascribed to the regions of relatively long separations where the force magnitude drops closely to zero. In addition, the present model is more accurate than the Huppmann-Riegger model when the liquid bridge gets stretched. Therefore, it is shown that the current model can give accurate prediction for liquid bridges between equal spheres.

6.2. Unequal spheres

In this section, results are presented to demonstrate the application of the present model to unequal spheres where the radii and contact angles are different. It is emphasized that the model developed in this study is able to treat such cases straightforwardly, while other analytical models have to turn to the effective radius and contact angle (Eq. (11)) based on the Derjaguin approximation.

The inset of Fig. 13(a) shows the asymmetric profile of a liquid bridge ($R_1 = 1$, $R_2 = 3$, $\theta_1 = 15°$, $\theta_2 = 60°$, $V = 0.04$) at separation $H = 0.1$. Similarly, the red markers show the optimal solution and the blue circle shows the model prediction. The inflection point on the concave profile shifts to the right side, indicating that more liquid is attracted by the left sphere with a smaller radius and contact angle. Fig. 13(a) plots the force of this liquid bridge. It is seen that the present model gives the best agreement with the optimal solution in comparison with other analytical models. The mean relative error is 3.1% with respect to the optimal solutions.

Fig. 13(b) shows another liquid bridge between unequal spheres ($R_1 = 2$, $R_2 = 1$, $\theta_1 = 120°$, $\theta_2 = 150°$, $V = 0.04$). The inset of the figure illustrates the bridge profile at distance $H = 0.2$, from which an asymmetric convex profile is observed. Again, from the force plot by Fig. 13(b), we find a superior performance of the present model. The mean relative error is 6.77% for $H/R \leq 0.2$. Beyond this separation, the force becomes small and the relative error increases, but the absolute error is not significant as indicated by the figure. The other models based on the Derjaguin approximation, despite their partly qualitative agreement with the optimal

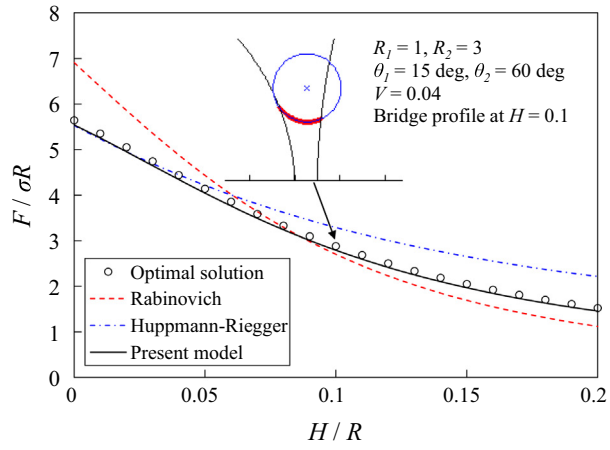

(a) $R_1 = 1$, $R_2 = 3$, $\theta_1 = 15°$, $\theta_2 = 60°$

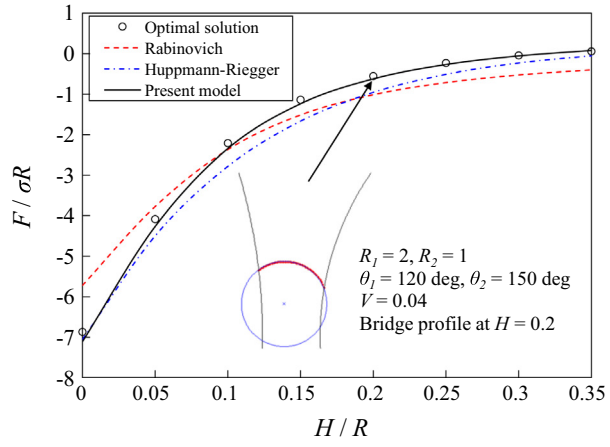

(b) $R_1 = 2$, $R_2 = 1$, $\theta_1 = 120°$, $\theta_2 = 150°$

Fig. 13. Liquid bridge forces between unequal spheres with $V = 0.04$. The insets show the bridge profiles at the conditions indicated by the arrows, for which the red lines illustrate the optimal solution and the blue circles are the model prediction. Note the characteristic radius $R = \min(R_1, R_2)$ herein. (For interpretation of the references to colour in this figure legend, the reader is referred to the web version of this article.)

solution, are not able to achieve the same accuracy. Hence, the proposed model can be used to calculate the force with high fidelity for general liquid bridge systems involving unequal spheres.

6.3. Bridges without a neck

As noted previously, not all liquid bridges have the neck or waist point to which the "gorge" method can be applied to calculate the force. In order to handle such bridges with highly asymmetric profiles, a correction method is proposed in Section 4.4, whose validity and necessity will be tested. Again, the Derjaguin approximation is used for other analytical models compared.

We consider a pair of unequal spheres for which the sphere radii, contact angles and liquid volume are $R_1 = 1$, $R_2 = 2$, $\theta_1 = 30°$, $\theta_2 = 120°$ and $V = 0.01$, respectively. Fig. 14(a) shows a representative profile of this liquid bridge at separation $H = 0.05$. It is clearly seen that, due to the large difference in contact angles, the center of the approximate circle is biased and its neck point lies inside the right sphere, which indicates that a true neck point is absent in this case. The comparison between various force models is given in Fig. 14(b). When the correction for neck position is used, the present model is in good agreement with the optimal solution (the mean relative error is 3.76%). It outperforms the Rabinovich equation and the Huppmann-Riegger model (using Derjaguin approximation) in accuracy. If this neck correction is inactivated, significant error is observed for the results.

Similar cases can be found in sphere-plane configurations as well. Fig. 15(a) gives an example with parameters: $R_1 = 1$, $\theta_1 = 60°$, $\theta_2 = 100°$ and $V = 0.1$. In the figure, the toroidal approximation of the bridge interface (blue arc) is only shown partially because of the large curvature radius, which is a good match for the optimal solution (red markers). Obviously, a waist point does not exist in this convex bridge, either. Fig. 15(b) plots the liquid bridge force against the sphere-plane distance. If the correction method is not used, the error grows with the distance and finally diverges, which may be ascribed to evaluating the interfacial curvature and capillary force at a false waist point. With the detection and correction of neck position, remarkable agreement with the optimal solution is restored again (the mean relative error is 0.47%). Therefore, the correction method proposed by this study can provide a more general solution for liquid bridge problems with significant improvement in the force calculation.

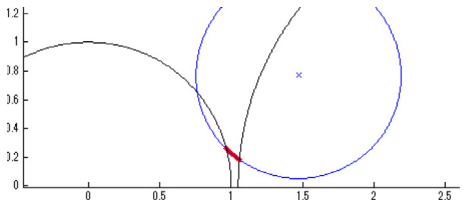

(a) Bridge profile at $H = 0.05$

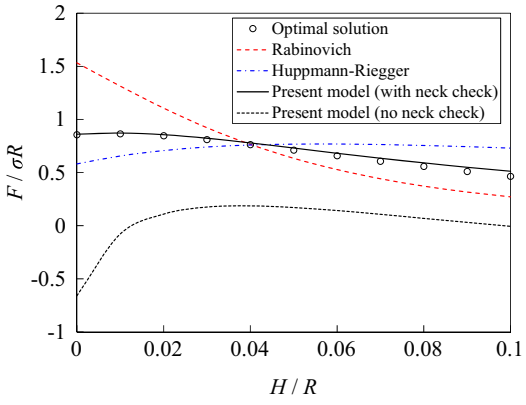

(b) Bridge force with respect to separation

Fig. 14. The profile and force of a sphere-sphere liquid bridge without neck point: $R_1 = 1$, $R_2 = 2$, $\theta_1 = 30°$, $\theta_2 = 120°$ and $V = 0.01$. (a) Representative profile at distance $H = 0.05$, in which the red markers are the optimal solution and the blue circle is the prediction by the present method. (b) Plot of capillary force, in which the result of uncorrected force calculation is also shown for comparison. Note the characteristic radius $R = \min(R_1, R_2)$ herein. (For interpretation of the references to colour in this figure legend, the reader is referred to the web version of this article.)

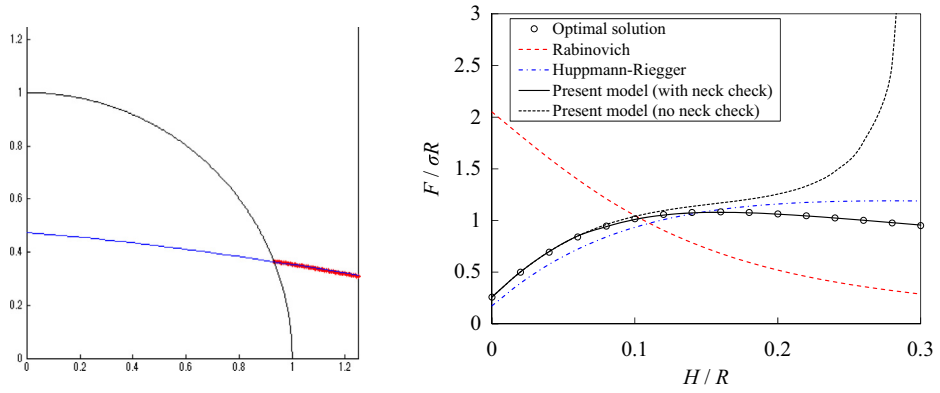

Fig. 15. The profile and force of a sphere-wall liquid bridge without neck point: $R_1 = 1$, $\theta_1 = 60°$, $\theta_2 = 100°$ and $V = 0.1$. (a) Representative profile at distance $H = 0.25$, in which the red markers are the optimal solution and the blue arc is the prediction by the present method. Note that the whole circle is too large to be fully included in this figure. (b) Plot of capillary force, in which the result of uncorrected force calculation is also shown for comparison. Note the characteristic radius $R = R_1$ herein. (For interpretation of the references to colour in this figure legend, the reader is referred to the web version of this article.)

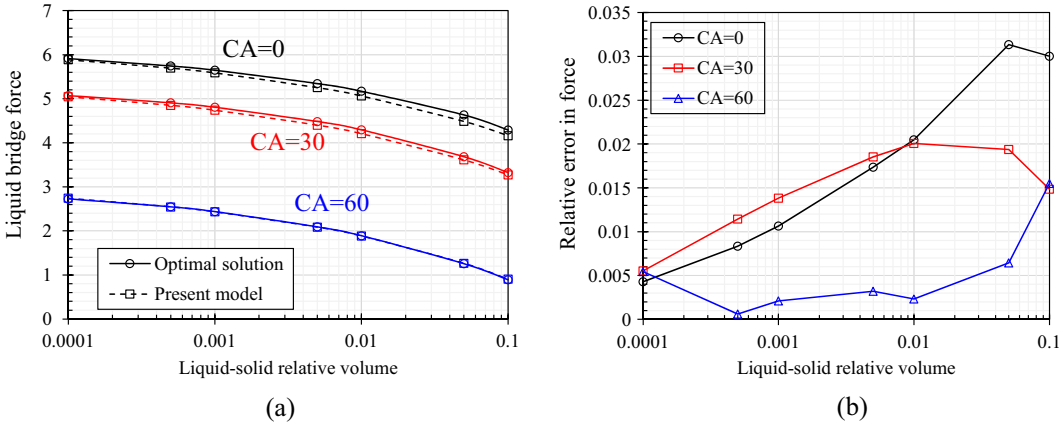

Fig. 16. Accuracy of force model at zero contact with contact angle (CA) of 0°, 30° and 60°: (a) force and (b) error. It implies that the relative error is below 4% for small CAs within the range of liquid volume tested (relative volume <0.1).

6.4. Accuracy at zero contact

The model based on toroidal approximation is mainly criticized for the violation of the constant curvature condition dictated by the Young-Laplace equation, see e.g. (Lian and Seville, 2016). Some numerical studies show that relative error due to the toroidal approximation is around 10% in general (Hotta et al., 1974; Orr et al., 1975), which is consistent with our results in preceding sections. The authors of Megias-Alguacil and Gauckler (2011) derived an equation of local error in the meniscus shape by inserting the approximate solution into the governing Young-Laplace formula. It is found that, the L^2-error norm of the circular profile reaches maximum at zero separation and decreases with the distance. Therefore, accuracy of the present model at close contact is examined in this section.

Fig. 16(a) shows the liquid bridge force as a function of the volume for two equal spheres with zero separation. The solid surfaces are hydrophilic, for which the contact angles are 0°, 30° and 60°, respectively. The liquid volume (relative to the particle volume) is varied within the range of $10^{-4} \leq V_L/(4\pi R^3/3) \leq 0.1$. The model prediction agrees with the optimal solution that is used as exact values. The relative error in the liquid bridge force, according to Fig. 16(b), is below 4% for all three error curves.

Fig. 17(b) shows the liquid bridge force for hydrophobic surfaces with contact angles of 90°, 120° and 150°. It is seen that the deviation of the model prediction from the optimal solution grows as the volume becomes larger. The trend of relative error in Fig. 17(b) implies basically a monotonic increase with respect to the liquid-solid volume ratio for those large contact angles. The maximum error is around 8% for contact angle of 150°. It seems that the slight deterioration of accuracy mainly comes from the error in curvature calculation for highly hydrophobic contact angles and large liquid volumes. The current results cohere with the error estimation by Megias-Alguacil and Gauckler (2011).

7. Conclusions

This study is dedicated to the modeling of capillary force arising from liquid bridges for spherical particles. The first part of this work presents an energetic approach by minimizing the interfacial energy to obtain the optimal solution of a static liquid bridge, which gives very exact values of the liquid bridge profile and force. This technique provides a powerful method for solving axisymmetric liquid bridge problems directly, and it also reveals many geometric and energetic aspects of the underlying system. The optimal solution is taken as reference data for the liquid bridge force in this study.

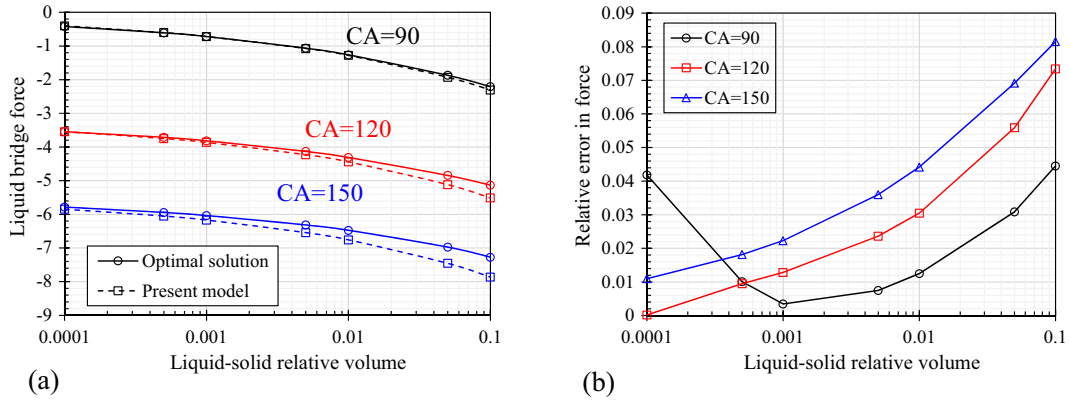

Fig. 17. Accuracy of force model at zero contact with contact angle (CA) of 90°, 120° and 150°: (a) force and (b) error. The relative error is below 10% for large CAs for relative liquid volume <0.1.

In the second part, a liquid bridge force model is developed based on the toroidal approximation of the interface shape. This model relates the embracing angle and the curvature radius to the fixed volume of the liquid. By solving those geometrical parameters, the capillary force can be calculated. Expressions are derived for both sphere-sphere and sphere-plane cases. In comparison with existing models, the proposed model has advantage in its generality, which is accurate for a wide range of liquid volumes, contact angles and radius ratios. The present model is validated against experimental data and optimal solutions in various configurations.

The proposed model would be useful in modeling inviscid capillary effects for spherical particles. In particular, it may be incorporated directly (or by pre-computing tabulated values for acceleration) into a productive DEM code to perform the numerical simulation of wet particle processing that are dominated mainly by the liquid bridge regime. The inter-particle force and the particle-wall liquid bridge force can thus be calculated accurately by using the model. Besides the capillary force, fully dynamic DEM simulations may involve the modeling of the bridge rupture (see Appendix B) and the liquid transfer (see e.g. (Shi and McCarthy, 2008; Washino et al., 2016)). The practical application and analytical refinement of the liquid bridge modeling is to be investigated in the future.

Finally, we would like to comment on some specific problems of liquid bridge modeling. As noted in the introduction, the present model, as well as many past studies (Chen et al., 2011; Huppmann and Riegger, 1975; Lian and Seville, 2016; Orr et al., 1975; Rabinovich et al., 2005; Willett et al., 2000), should be attributed to the solution in the constant-volume scenario of liquid bridge problems. This approach is useful for involatile liquids and immiscible liquid-liquid emulsions. For volatile liquids, it is desirable to take the mass diffusion through the vapor phase into account. The constant pressure approach may be employed if the diffusion prevails. In that case, some equations developed in this study can still be used to approximate the bridge geometry and volume in a straightforward manner. On the other hand, if the characteristic diffusive time scale is to be resolved, the modeling of the transport behavior through the background vapor becomes necessary (see e.g. (Cheng and Wang, 2012; Mani et al., 2015)). Anyway, the present model should be still applicable to those "diffusive" liquid bridges, provided that they remains mechanically quasi-equilibrium owing to the dominant capillary effect. In addition, it is noted that a microscopic liquid bridge system may involve other interactions besides the capillary force. Among them, the disjoining pressure might be important at close distance for non-spherical solid tips (Gao, 1997; Willett et al., 2000). The van der Waals force may exist between adhesive particles; the electrical double-layer force may also arise within the meniscus depending on the surface properties of the solid particle. However, in general, they are considered to be insignificant with the existence of capillary forces (Butt et al., 2006).

Acknowledgements

This research was supported by the Initiatives for Atomic Energy Basic and Generic Strategic Research of the Ministry of Education, Culture, Science and Technology of Japan.

Appendix A

The derivation of the initial guess (35) for the iterative solving is explained as follows. We assume that the bridge is a straight pipe connecting the solid surfaces. Therefore, the following equations are self-explanatory with the cylindrical radius b and liquid volume V:

$$\begin{aligned} &b \equiv R_1 \sin\alpha_1 = R_2 \sin\alpha_2 \\ &V = \pi b^2 (H + R_1(1-\cos\alpha_1) + R_2(1-\cos\alpha_2)) - V_1 - V_2 \end{aligned} \tag{43}$$

The spherical cap volumes V_1 and V_2 are given by Eq. (19). In order to simplify the expressions, we take the Taylor expansion of trigonometric functions to the lowest-order non-constant terms:

$$\begin{aligned} &\sin\alpha \approx \alpha \\ &\cos\alpha \approx 1 - \alpha^2/2 \end{aligned} \tag{44}$$

Inserting those into the equations and dropping all high-order terms, a quartic equation is obtained:

$$\frac{1}{4}(1 + R_1/R_2)\alpha_1^4 + \frac{H}{R_1}\alpha_1^2 - \frac{V}{\pi R_1^3} = 0 \tag{45}$$

It has one positive root as given by Eq. (35). The initial guess for the sphere-plane case can be determined easily in a similar fashion.

Appendix B

We discuss how the critical rupture distance H_c of a liquid bridge could be located by using the optimization technique developed in Section 3. According to the past studies (Lian et al., 1993; Pepin et al., 2000), the stability of a static liquid bridge solution is determined by the energetic variation in total free energy with respect to perturbations. Since our optimal solution is also based on the energetic description, it is reasonable to postulate that the

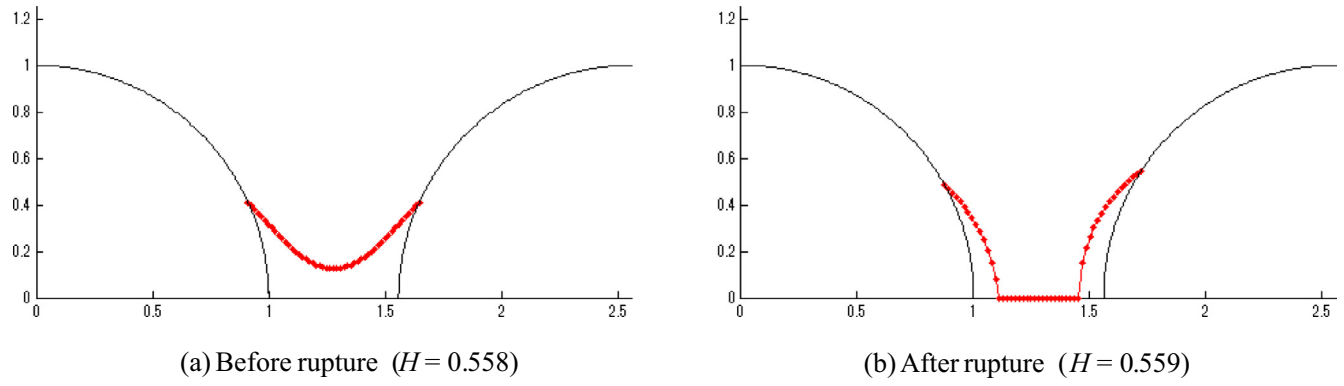

Fig. 18. Rupture of a static liquid bridge with $V = 0.1$ and $\theta = 10°$. Optimal solutions are shown for separations (a) $H = 0.558$ (pre-rupture) and (b) $H = 0.559$ (post-rupture). It is seen that a dramatic change occurs by a small increment $\Delta H = 10^{-3}$ in separation, which indicates a pull-off of the liquid bridge at the current distance.

current procedure can identify stable and unstable states by yielding different final solutions: stable states are retained in bridge forms and unstable states leads to separated droplets. This has been empirically tested in the present study. The resulting sphere-sphere rupture distances are compared with the equation of Lian et al. (1993) which is neatly proportional to the cubic root of the liquid volume:

$$H_{c,sphere-sphere} = (1 + 0.5\theta) \cdot V^{1/3} \tag{46}$$

For the sphere-plane case, the power-law relationship of Mikami et al. (1998) is considered:

$$H_{c,sphere-plane} = (0.95 + 0.22\theta) \cdot V^{0.32} \tag{47}$$

For a liquid bridge with volume V and contact angle θ fixed, we begin with some initial separation distance H by which the solution is assured to be stable. Then the separation H is elongated by ΔH incrementally and the solution is updated and examined. An example is given in Fig. 18 for equal spheres with $R = 1$, $V = 0.1$ and $\theta = 10°$. By increasing the distance by $\Delta H = 0.001$ each time, we find that the solution suddenly changes at some point. Fig. 18(a, b) show the pre- and post-rupture solutions obtained at $H = 0.558$ and $H = 0.559$, respectively. It is thus inferred that the optimal solution can be no longer found as a bridge beyond the current distance. Consequently, the rupture distance can be determined (coming with a small uncertainty ΔH). The sudden rupture within a very small variation of distance shown in Fig. 18 is consistent with the comment by de Boer and de Boer (2007) that static solutions of liquid bridge break down at finite neck and nonzero force. In fact, recent dynamic simulations of liquid bridge systems (Darabi et al., 2010; Sun and Sakai, 2016) figured out a fast and irreversible thinning of the neck during the rupture.

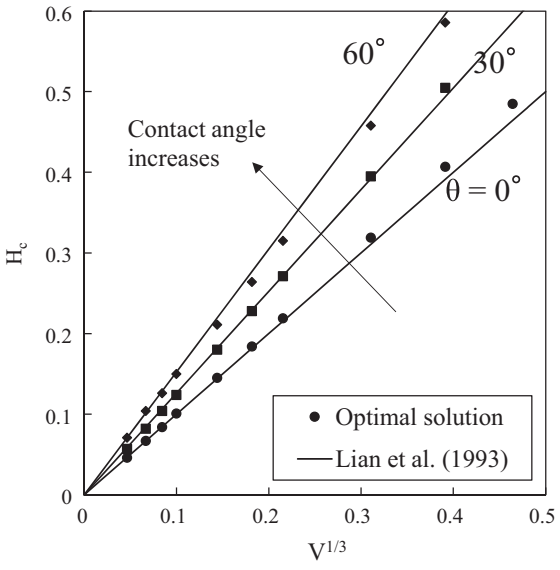

Fig. 19. Rupture distance of liquid bridge between two spheres. Numerical results are compared with the empirical model of Lian et al. (1993).

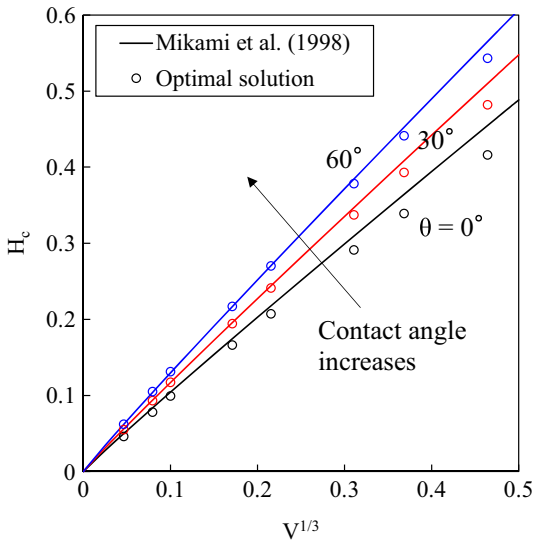

Fig. 20. Rupture distance of liquid bridge between sphere and plane. Numerical results are compared with the fitting equation of Mikami et al. (1998).

By using the approach described above, we are able to find interactively the rupture distance of liquid bridge between two equal spheres. Tests are carried out for contact angles of 0°, 30°, and 60°, respectively. The results are shown in Fig. 19 with respect to the liquid volume, which is in good agreement with Lian's formula (46). Similarly, Fig. 20 shows the rupture distance in a sphere-plane configuration. The agreement with Mikami's fitting equation (47) is also reasonable.

Appendix C. Supplementary material

Some MATLAB scripts are provided to help the readers to compute the liquid bridge interactions. They are implementations of the interface optimizer and the liquid bridge force model described

in the paper. Some driver routines are provided to show their usage. More information are available in the readme file included in the package. The programs are developed and tested with the MATLAB R2013a version. Supplementary data associated with this article can be found, in the online version, at https://doi.org/10.1016/j.ces.2018.02.034.

References

Ardito, R., Corigliano, A., Frangi, A., Rizzini, F., 2014. Advanced models for the calculation of capillary attraction in axisymmetric configurations. Eur. J. Mech. – A/Solids 47, 298–308. https://doi.org/10.1016/j.euromechsol.2014.05.002.

Balakin, B.V., Kutsenko, K.V., Lavrukhin, A.A., Kosinski, P., 2015. The collision efficiency of liquid bridge agglomeration. Chem. Eng. Sci. 137, 590–600. https://doi.org/10.1016/j.ces.2015.07.002.

Brakke, K.A., 1992. The surface evolver. Exp. Math. 1, 141–165. https://doi.org/10.1080/10586458.1992.10504253.

Broesch, D.J., Frechette, J., 2012. From concave to convex: capillary bridges in slit pore geometry. Langmuir 28, 15548–15554. https://doi.org/10.1021/la302942k.

Butt, H.J., Farshchi-Tabrizi, M., Käppl, M., 2006. Using capillary forces to determine the geometry of nanocontacts. J. Appl. Phys. 100, 24312. https://doi.org/10.1063/1.2210188.

Chen, Y., Zhao, Y., Gao, H., Zheng, J., 2011. Liquid bridge force between two unequal-sized spheres or a sphere and a plane. Particuology 9, 374–380. https://doi.org/10.1016/j.partic.2010.11.006.

Cheng, T.-L., Wang, Y.U., 2012. Spontaneous formation of stable capillary bridges for firming compact colloidal microstructures in phase separating liquids: a computational study. Langmuir 28, 2696–2703. https://doi.org/10.1021/la2044152.

Cundall, P.A., Strack, O.D.L., 1979. A discrete numerical model for granular assemblies. Géotechnique 29, 47–65. https://doi.org/10.1680/geot.1979.29.1.47.

Darabi, P., Li, T., Pougatch, K., Salcudean, M., Grecov, D., 2010. Modeling the evolution and rupture of stretching pendular liquid bridges. Chem. Eng. Sci. 65, 4472–4483. https://doi.org/10.1016/j.ces.2010.04.003.

de Boer, M.P., de Boer, P.C.T., 2007. Thermodynamics of capillary adhesion between rough surfaces. J. Colloid Interface Sci. 311, 171–185. https://doi.org/10.1016/j.jcis.2007.02.051.

Dörmann, M., Schmid, H.-J., 2014. Simulation of capillary bridges between nanoscale particles. Langmuir 30, 1055–1062. https://doi.org/10.1021/la404409k.

Farmer, T.P., Bird, J.C., 2015. Asymmetric capillary bridges between contacting spheres. J. Colloid Interface Sci. 454, 192–199. https://doi.org/10.1016/j.jcis.2015.04.045.

Fisher, R.A., 1926. On the capillary forces in an ideal soil; correction of formulae given by W.B. Haines. J. Agric. Sci. 16, 492. https://doi.org/10.1017/S0021859600007838.

Gao, C., 1997. Theory of menisci and its applications. Appl. Phys. Lett. 71, 1801–1803. https://doi.org/10.1063/1.119403.

Georgiev, M.T., Danov, K.D., Kralchevsky, P.A., Gurkov, T.D., Krusteva, D.P., Arnaudov, L.N., Stoyanov, S.D., Pelan, E.G., 2018. Rheology of particle/water/oil three-phase dispersions: electrostatic vs. capillary bridge forces. J. Colloid Interface Sci. 513, 515–526. https://doi.org/10.1016/j.jcis.2017.11.057.

Girardi, M., Radl, S., Sundaresan, S., 2016. Simulating wet gas-solid fluidized beds using coarse-grid CFD-DEM. Chem. Eng. Sci. 144, 224–238. https://doi.org/10.1016/j.ces.2016.01.017.

Gladkyy, A., Schwarze, R., 2014. Comparison of different capillary bridge models for application in the discrete element method. Granul. Matter 16, 911–920. https://doi.org/10.1007/s10035-014-0527-z.

Harireche, O., Faramarzi, A., Alani, A.M., 2013. A toroidal approximation of capillary forces in polydisperse granular assemblies. Granul. Matter 15, 573–581. https://doi.org/10.1007/s10035-013-0425-9.

Heady, R.B., Cahn, J.W., 1970. An analysis of the capillary forces in liquid-phase sintering of spherical particles. Metall. Trans. 1, 185–189. https://doi.org/10.1007/BF02819260.

Hotta, K., Takeda, K., Iinoya, K., 1974. The capillary binding force of a liquid bridge. Powder Technol. 10, 231–242. https://doi.org/10.1016/0032-5910(74)85047-3.

Huppmann, W., Riegger, H., 1975. Modelling of rearrangement processes in liquid phase sintering. Acta Metall. 23, 965–971. https://doi.org/10.1016/0001-6160(75)90010-3.

Israelachvili, J.N., 2010. Intermolecular and Surface Forces. Academic Press.

Jarray, A., Magnanimo, V., Ramaioli, M., Luding, S., 2017. Scaling of wet granular flows in a rotating drum. In: Radjai, F., Nezamabadi, S., Luding, S., Delenne, J.Y. (Eds.), EPJ Web of Conferences. EDP Sciences, p. 3078. doi:10.1051/epjconf/201714003078.

Kan, H., Nakamura, H., Watano, S., 2015. Numerical simulation of particle–particle adhesion by dynamic liquid bridge. Chem. Eng. Sci. 138, 607–615. https://doi.org/10.1016/j.ces.2015.08.043.

Lambert, P., Chau, A., Delchambre, A., Régnier, S., 2008. Comparison between two capillary forces models. Langmuir 24, 3157–3163. https://doi.org/10.1021/la7036444.

Lambert, P., Delchambre, A., 2005. Parameters ruling capillary forces at the submillimetric scale. Langmuir 21, 9537–9543. https://doi.org/10.1021/la0507131.

Lian, G., Seville, J., 2016. The capillary bridge between two spheres: new closed-form equations in a two century old problem. Adv. Colloid Interface Sci. https://doi.org/10.1016/j.cis.2015.11.003.

Lian, G., Thornton, C., Adams, M.J., 1993. A theoretical study of the liquid bridge forces between two rigid spherical bodies. J. Colloid Interface Sci. 161, 138–147. https://doi.org/10.1006/jcis.1993.1452.

Liu, P.Y., Yang, R.Y., Yu, A.B., 2013. DEM study of the transverse mixing of wet particles in rotating drums. Chem. Eng. Sci. 86, 99–107. https://doi.org/10.1016/j.ces.2012.06.015.

Liu, P.Y., Yang, R.Y., Yu, A.B., 2011. Dynamics of wet particles in rotating drums: effect of liquid surface tension. Phys. Fluids 23, 13304. https://doi.org/10.1063/1.3543916.

Mani, R., Semprebon, C., Kadau, D., Herrmann, H.J., Brinkmann, M., Herminghaus, S., 2015. Role of contact-angle hysteresis for fluid transport in wet granular matter. Phys. Rev. E 91, 42204. https://doi.org/10.1103/PhysRevE.91.042204.

Megias-Alguacil, D., Gauckler, L.J., 2011. Accuracy of the toroidal approximation for the calculus of concave and convex liquid bridges between particles. Granul. Matter 13, 487–492. https://doi.org/10.1007/s10035-011-0260-9.

Mikami, T., Kamiya, H., Horio, M., 1998. Numerical simulation of cohesive powder behavior in a fluidized bed. Chem. Eng. Sci. 53, 1927–1940. https://doi.org/10.1016/S0009-2509(97)00325-4.

Mitarai, N., Nori, F., 2006. Wet granular materials. Adv. Phys. 55, 1–45. https://doi.org/10.1080/00018730600626065.

Mitchell, W.R., Forny, L., Althaus, T., Dopfer, D., Niederreiter, G., Palzer, S., 2017. Compaction of food powders: the influence of material properties and process parameters on product structure, strength, and dissolution. Chem. Eng. Sci. 167, 29–41. https://doi.org/10.1016/j.ces.2017.03.056.

Neidinger, R.D., 2010. Introduction to automatic differentiation and MATLAB object-oriented programming. SIAM Rev. 52, 545–563. https://doi.org/10.1137/080743627.

Orr, F.M., Scriven, L.E., Rivas, A.P., Bradford, E.B., 1975. Pendular rings between solids: meniscus properties and capillary force. J. Fluid Mech. 67, 723. https://doi.org/10.1017/S0022112075000572.

Payam, A.F., Fathipour, M., 2011. A capillary force model for interactions between two spheres. Particuology 9, 381–386. https://doi.org/10.1016/j.partic.2010.11.004.

Pepin, X., Rossetti, D., Iveson, S., Simons, S., 2000. Modeling the evolution and rupture of pendular liquid bridges in the presence of large wetting hysteresis. J. Colloid Interface Sci. 232, 289–297. https://doi.org/10.1006/jcis.2000.7182.

Press, W.H., Teukolsky, S.A., Vetterling, W.T., Flannery, B.P., 2007. Numerical Recipes third ed.: The Art of Scientific Computing. Cambridge University Press.

Rabinovich, Y.I., Esayanur, M.S., Moudgil, B.M., 2005. Capillary forces between two spheres with a fixed volume liquid bridge: theory and experiment. Langmuir 21, 10992–10997. https://doi.org/10.1021/la0517639.

Remy, B., Khinast, J.G., Glasser, B.J., 2012. Wet granular flows in a bladed mixer: experiments and simulations of monodisperse spheres. AIChE J. 58, 3354–3369. https://doi.org/10.1002/aic.13743.

Shi, D., McCarthy, J.J., 2008. Numerical simulation of liquid transfer between particles. Powder Technol. 184, 64–75. https://doi.org/10.1016/j.powtec.2007.08.011.

Shigeto, Y., Sakai, M., 2013. Arbitrary-shaped wall boundary modeling based on signed distance functions for granular flow simulations. Chem. Eng. J. 231, 464–476.

Soulié, F., Cherblanc, F., El Youssoufi, M.S., Saix, C., 2006. Influence of liquid bridges on the mechanical behaviour of polydisperse granular materials. Int. J. Numer. Anal. Methods Geomech. 30, 213–228. https://doi.org/10.1002/nag.476.

Sun, X., Sakai, M., 2016. Direct numerical simulation of gas-solid-liquid flows with capillary effects: an application to liquid bridge forces between spherical particles. Phys. Rev. E 94, 63301. https://doi.org/10.1103/PhysRevE.94.063301.

Sun, X., Sakai, M., 2015. Three-dimensional simulation of gas–solid–liquid flows using the DEM–VOF method. Chem. Eng. Sci. 134, 531–548. https://doi.org/10.1016/j.ces.2015.05.059.

Sun, X., Sakai, M., Sakai, M.-T., Yamada, Y., 2014. A Lagrangian-Lagrangian coupled method for three-dimensional solid–liquid flows involving free surfaces in a rotating cylindrical tank. Chem. Eng. J. 246, 122–141. https://doi.org/10.1016/j.cej.2014.02.049.

Tang, T., He, Y., Tai, T., Wen, D., 2017. DEM numerical investigation of wet particle flow behaviors in multiple-spout fluidized beds. Chem. Eng. Sci. 172, 79–99. https://doi.org/10.1016/j.ces.2017.06.025.

Tegzes, P., Vicsek, T., Schiffer, P., 2003. Development of correlations in the dynamics of wet granular avalanches. Phys. Rev. E 67, 17. https://doi.org/10.1103/PhysRevE.67.051303.

Tsunazawa, Y., Fujihashi, D., Fukui, S., Sakai, M., Tokoro, C., 2016. Contact force model including the liquid-bridge force for wet-particle simulation using the discrete element method. Adv. Powder Technol. 27, 652–660. https://doi.org/10.1016/j.apt.2016.02.021.

Wang, L., Su, F., Xu, H., Rong, W., Xie, H., 2016. Capillary bridges and capillary forces between two axisymmetric power–law particles. Particuology 27, 122–127. https://doi.org/10.1016/j.partic.2015.08.005.

Wang, Y., Michielsen, S., Lee, H.J., 2013. Symmetric and asymmetric capillary bridges between a rough surface and a parallel surface. Langmuir 29, 11028–11037. https://doi.org/10.1021/la401324f.

Washino, K., Miyazaki, K., Tsuji, T., Tanaka, T., 2016. A new contact liquid dispersion model for discrete particle simulation. Chem. Eng. Res. Des. 110, 123–130. https://doi.org/10.1016/j.cherd.2016.02.022.

Washino, K., Tan, H.S., Hounslow, M.J., Salman, A.D., 2013. A new capillary force model implemented in micro-scale CFD–DEM coupling for wet granulation. Chem. Eng. Sci. 93, 197–205. https://doi.org/10.1016/j.ces.2013.02.006.

Willett, C.D., Adams, M.J., Johnson, S.A., Seville, J.P.K., 2000. Capillary bridges between two spherical bodies. Langmuir 16, 9396–9405. https://doi.org/10.1021/la000657y.

Yang, L., Tu, Y., Fang, H., 2010. Modeling the rupture of a capillary liquid bridge between a sphere and plane. Soft Matter 6, 6178. https://doi.org/10.1039/c0sm00497a.

Zhou, F., Ma, Q., 2016. Exact solution for capillary interactions between two particles with fixed liquid volume. Appl. Math. Mech. 37, 1597–1606. https://doi.org/10.1007/s10483-016-2142-8.